Accretion Disks: An Overview

Bergur Halldórsson

Faculty of Physics
University of Iceland
2017

ACCRETION DISKS: AN OVERVIEW

Bergur Halldórsson

16 ECTS thesis submitted in partial fulfillment of a
Baccalaureus Scientiæ degree in Physics

Advisor
Gunnlaugur Björnsson

Faculty of Physics
School of Engineering and Natural Sciences
University of Iceland
Reykjavik, May 2017

Accretion Disks: An Overview
16 ECTS thesis submitted in partial fulfillment of a B.Sc. degree in Physics

Faculty of Physics
School of Engineering and Natural Sciences
University of Iceland
Hjarðarhagi 2-6
107, Reykjavik, Reykjavik
Iceland

Telephone: 525 4000

Bibliographic information:
Bergur Halldórsson, 2017, Accretion Disks: An Overview, B.Sc. thesis, Faculty of Physics, University of Iceland.

Abstract

Accretion disks are complex systems which are not yet entirely understood. Here a short overview is given of accretion disk theory, describing the disks, the thin disk approximation to simplify calculations and a description of the α-disk model. The Eddington limit and its role in accretion disks is discussed. Newtonian and Pseudo-Newtonian gravitational potentials are introduced and analyzed. Modeling black hole systems is also covered. Finally, observations of four systems possessing black holes are discussed.

Contents

List of Figures

1 Introduction

Accretion is a process whereby matter accumulates and forms a disk-like structure due to gravity and sometimes also forms a massive object. It is one of the processes largely responsible for the appearance of most objects in the universe. Almost all astronomical objects, from planets and stars to entire galaxies were formed through this process. It also powers some of the most energetic phenomena observed in the universe. Generally, accreting matter forms a disk around a central object due to the conservation of the matter's angular momentum. We will look at the dynamics of these disks, both generally and using a thin disk approximation as well as commonly used gravitational potentials.

We will also discuss several systems that are interpreted as compact objects possessing an accretion disk: Cygnus X-1, an extensively studied X-ray binary system, SS 433, another binary known for its disk's and jets' precession, Sagittarius A*, the supermassive black hole at the center of our galaxy, and M104, a spiral galaxy possessing an unusually large black hole at its center.

2 Accretion Disks

Particles caught by a massive object's gravitational pull rarely happens to be travelling directly towards the object. It generally has some angular momentum which it must lose in order to fall further inwards. Looking at the angular momentum for a circular orbit, $L = mvr$, we see that in order for r to decrease, L must decrease, assuming that the mass is constant. As momentum must be conserved, it can only be transferred elsewhere. It turns out that the angular momentum in accretion is transferred via friction and moves outwards as most of the matter making up the disk moves inwards. Here we will consider basic accretion disk theory. Our discussion is largely adapted from [16], [5] and [18].

Let's look at the mechanics of these disks more closely. Due to the shape of the disk it is best to use cylindrical coordinates, in which z is the vertical distance from the equatorial plane and r is the radial distance from the z-axis. At the center of the coordinate system we have a massive object with a spherically symmetric gravitational field. The gravitational potential Φ is dependent on the distance from the coordinate system's center, $r = \sqrt{R^2 + z^2}$, and obeys the following:

$$\Phi(r) < 0, \tag{2.1}$$

the potential must be negative everywhere, obviously the gravitational field cannot repel objects from the center anywhere,

$$\frac{d\Phi}{dr} > 0, \tag{2.2}$$

it must be strongest at the center and weakens as r increases. We require that $r = 0$ must be the only critical point, and the potential must go to 0 as r approaches infinity,

$$\Phi(r)_{r \longrightarrow \text{inf}} \longrightarrow 0. \tag{2.3}$$

Two potentials will be explored in this thesis, the familiar Newtonian potential,

$$\Phi_N(r) = -\frac{GM}{r}, \tag{2.4}$$

and a pseudo-Newtonian potential,

$$\Phi_{PN}(r) = -\frac{GM}{r - r_g}, \tag{2.5}$$

where $r_g = 2GM/c^2$ is the gravitational radius of the central object and where the singularity has been shifted out to $r = r_g$ [16].

2.1 Disk formation

We should start by answering an important question: why does accreting matter so commonly form a disk rather than, for instance, staying spherically symmetrical?

It is due to the angular momentum of the matter forming the disk. Each particle has its own angular momentum, $\vec{L} = \vec{r} \times m\vec{v}$ where $\vec{r}$ is the position vector of the particle relative to the center of the coordinate system and $\vec{v}$ is its velocity vector. The sum of the angular momentum vectors of all the particles is conserved, even during collisions or other interactions. It is extremely unlikely that the total angular momentum will be equal to 0. This means that the angular momentum vector will point in a specific direction, which is perpendicular to the position and velocity vectors and the plane in which the disk forms. As collisions occur in the matter, the angular momenta of individual particles will come closer to the average, bringing their orbits into the plane perpendicular to the total angular momentum.

2.2 Accretion disks in binary systems

Accretion disks can form in binary systems under certain circumstances. The more massive body will, during its evolution, expand past its Roche lobe, the region in a binary system within which matter is gravitationally bound to that object. The outermost particles will then flow through the L_1 Lagrangian point and form a disk around the other body. The donor body is generally a giant, since it has to have a

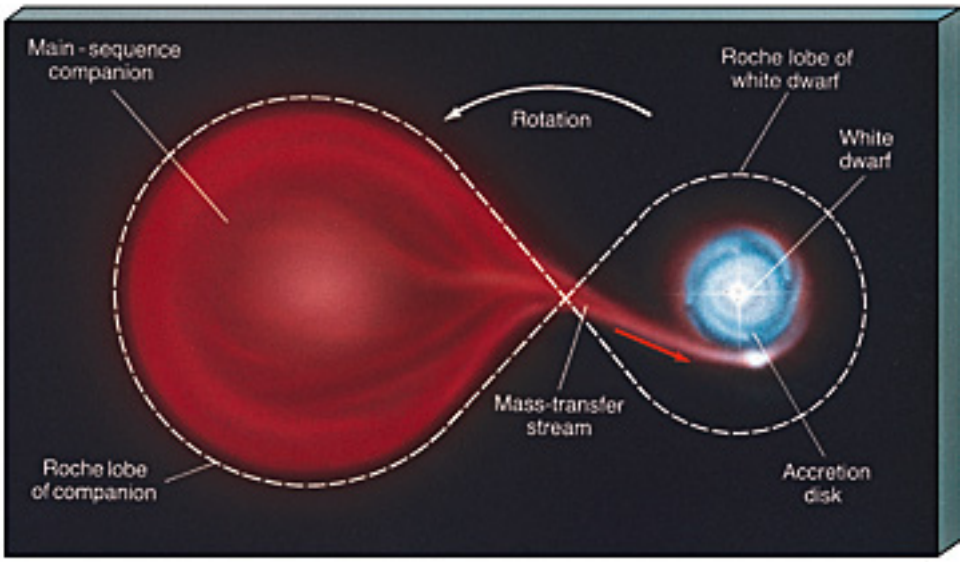

Figure 2.1: Binary system made up of a red giant and white dwarf. The Roche lobes are shown by the dashed line, the L_1 Lagrangian point is the intersection where the lobes meet [9].

large enough volume to reach the Roche lobe. The other body in this type of system may be a white dwarf, neutron star or black hole. [9]

2.3 Adiabatic Accretion

If we consider the Newtonian potential $\Phi_N = -GM/r$, when gas falls from r_0 to r, gravitational potential energy is converted to kinetic energy. The amount of energy converted is $\Delta\Phi = -GM(1/r - 1/r_0)$ which, if $r_0 \gg r$, can be simplified as $\Delta\Phi = -GM/r$. If the gas is at rest or in a circular Kepler orbit by the end of infall then the amount of energy dissipated per unit mass is

$$e = -\frac{GM}{r}, \tag{2.6}$$

at rest or

$$e = \Phi + \frac{v^2}{2} = -\frac{GM}{r} + \frac{1}{2}\frac{GM}{r} = -\frac{GM}{2r}, \tag{2.7}$$

for the Kepler orbit, using $v = \sqrt{r d\Phi/dr}$ for the Newtonian potential.

The energy dissipated ends up as internal energy of the gas and in radiation. We will look specifically at adiabatic accretion, in which the loss of energy due to radiation is neglected.

If the gas being accreted is an ideal gas with a constant ratio of specific heats, γ, then the internal energy per unit mass is

$$e = -\frac{P}{(\gamma - 1)\rho}. \tag{2.8}$$

Here P is the gas pressure, given by $P = \mathcal{R}\rho T/\mu$, using the gas constant $\mathcal{R}$ and the mean atomic weight per particle μ. If the gas goes into a circular orbit, we can find the temperature of the gas after the dissipation has taken place using

$$T = \frac{1}{2}(\gamma - 1)T_{vir}, \tag{2.9}$$

where T_{vir} is the virial temperature [18],

$$T_{vir} = \frac{GM\mu}{Rr}. \tag{2.10}$$

2.4 Analysis of accretion disks using Navier-Stokes

The following discussion is adapted from [5]. We use the Navier-Stokes equations to describe the motion of a viscous compressible fluid with a variable dynamic viscosity ν and a bulk viscosity coefficient equal to zero. If we have a fixed volume V element within a surface S and fluid density ρ then the rate of the fluid mass change in the volume is

$$\frac{\partial}{\partial t}\int_V \rho dV. \tag{2.11}$$

If there is no source or sink for matter within the volume, this must be equal to the total mass inflow integrated over the surface of the volume. The mass flow outward across an element $d\vec{S}$ can be expressed as $\rho\vec{v} \cdot d\vec{S}$ where $\vec{v}$ is the fluid's velocity

vector. We can then use

$$-\int_S \rho\vec{v}\cdot d\vec{S} = -\int_V \nabla\cdot(\rho\vec{v})dV, \tag{2.12}$$

which gives the mass gained by volume. We now have the mass flow outward in eq. (2.12) and the mass gained by volume. Setting these as equal, we obtain,

$$\frac{\partial}{\partial t}\int_V \rho dV = -\int_V \nabla\cdot(\rho\vec{v})dV, \tag{2.13}$$

which gives the mass conservation law,

$$\frac{\partial}{\partial t}\rho + \nabla\cdot(\rho\vec{v}) = 0. \tag{2.14}$$

We then try to find a similar conservation law for momentum. To do this, we define forces acting on the fluid element, external volume forces f_e, and internal volume forces f_i. In order to accurately describe the internal forces, we must use a viscous stress tensor,

$$\tau_{ij} = \mu\sigma_{ij} = \mu\Big((\partial_i v_j + \partial_j v_i) - \frac{2}{3}(\nabla\cdot v)\partial_{ij}\Big). \tag{2.15}$$

Here, σ_{ij} is the shear tensor and μ is the fluid's dynamic viscosity. We then also use the stress tensor,

$$\Upsilon = -PI + \tau, \tag{2.16}$$

where P is the pressure, I is the identity matrix and τ is the viscous stress tensor defined above [5].

From here we can find the internal forces $f_i = \nabla\cdot\Upsilon = -\nabla P + \nabla\cdot\tau$. In addition, we can also find the external forces $f_e = -\nabla\Phi$, assuming those forces come from the gravitational potential Φ only.

We use all this to get the following equation of momentum conservation,

$$\rho\Big(\frac{\partial}{\partial t}\vec{v} + (\vec{v}\cdot\nabla)\vec{v}\Big) = \nabla\Upsilon + \rho f_e = -\nabla P + \nabla\cdot\tau - \rho\Delta\Phi, \tag{2.17}$$

which is the Navier-Stokes equation of motion. When dealing with accretion disks, it is generally best to use cylindrical coordinates as mentioned above, both due to the shape of the disk and to simplify integrations. We will assume that the disk's properties do not change based on the φ coordinate so $\frac{\partial}{\partial\varphi} = 0$. The z coordinate can also be ignored by assuming that the disk is symmetric with respect to the equatorial plane and integrating through the depth of the disk. This simplifies the problem and we end up with the velocity components,

$$v_r(r, z) \simeq v_r(r), \tag{2.18}$$

$$v_\varphi(r, z) \simeq v_\varphi(r), \tag{2.19}$$

$$v_z \simeq 0. \tag{2.20}$$

We now define the surface density by integrating the density over the disk's vertical thickness,

$$\Sigma = \int_{-z_0}^{z_0} \rho dz, \tag{2.21}$$

where z_0 equals half the vertical width.

We also integrate the viscous stress tensor $\tau_{\mu\nu}$ over the vertical width of the disk to get $T_{\mu\nu}$,

$$T_{\mu\nu} = \int_{-z_0}^{z_0} \tau_{\mu\nu} dz. \tag{2.22}$$

The equation describing radial transport is then

$$\frac{\partial v_r}{\partial t} + v_r \frac{\partial v_r}{\partial r} = -\frac{1}{\Sigma(t, r)} \frac{\partial P}{\partial r} + \frac{v_\varphi^2}{r} - \frac{\partial \Phi}{\partial r} + a_r^{visc}, \tag{2.23}$$

where a_r^{visc} is the acceleration due to the viscosity in the radial direction. This equation can be simplified with two approximations. First, we neglect the gas gradient pressure in the radial direction. Second, we assume that two of the components

of the viscous stress tensor $T_{\mu\nu}$, i.e. T_{rr} and $T_{r\varphi}$ are both equal to 0 and therefor $a_r^{visc} = 0$ as well. This simplifies eq. (2.23) and it now becomes

$$\frac{\partial v_r}{\partial t} + v_r \frac{\partial v_r}{\partial r} = \frac{v_\varphi^2}{r} - \frac{\partial \Phi_T}{\partial r}. \tag{2.24}$$

Here, Φ_T is the gravitational potential of both the central object and the disk itself and is both a function of radius and time, due to the infall of matter.

Looking at the motion of matter in the φ direction, we can get, based on the Navier-Stokes equation of motion, eq. (2.17),

$$\frac{\partial v_\varphi}{\partial t} + v_r \frac{\partial v_\varphi}{\partial r} + \frac{v_r v_\phi}{r} = a_\varphi^{visc}. \tag{2.25}$$

The acceleration in the radial and azimuthal directions due to viscosity is given by

$$a_r^{visc} = \frac{1}{r\Sigma(t,r)}\Big(\frac{\partial(rT_{rr})}{\partial r} - T_{\varphi\varphi}\Big), \tag{2.26}$$

$$a_\varphi^{visc} = \frac{1}{r\Sigma(t,r)}\Big(\frac{\partial(rT_{r\varphi})}{\partial r}\Big), \tag{2.27}$$

where the T terms are given by,

$$T_{rr} = 2\nu\Sigma(t,r)\Big[\frac{\partial v_r}{\partial r} - \frac{1}{3}\nabla\cdot\vec{v}\Big], \tag{2.28}$$

$$T_{\varphi\varphi} = 2\nu\Sigma(t,r)\Big[\frac{v_r}{r} - \frac{1}{3}\nabla\cdot\vec{v}\Big], \tag{2.29}$$

$$T_{r\varphi} = \nu\Sigma(t,r)\Big[r\frac{\partial}{\partial r}\big(\frac{v_\varphi}{r}\big)\Big], \tag{2.30}$$

and are the components of the vertically integrated viscous stress tensor for cylindrical coordinates. The divergence of the velocity field is given by [5]

$$\nabla\cdot\vec{v} = \frac{1}{r}\frac{\partial}{\partial r}(rv_r). \tag{2.31}$$

If the left side of that equation is equal to zero, then the fluid is incompressible. In our case however, the fluid is compressible.

3 Thin Disk Approximation

This chapter is largely adapted from [16]. The sections on the scale of height and the α-disk model are adapted from [5].

Let's assume that $z_0 \ll r$ for an accretion disk. In that case the rotational velocity of matter within the disk is defined purely by the distance r from the center and we can look at the disk as a series of concentric cylinders with constant radii [16]. The surface mass density was defined in eq. (2.21).

If the matter in the disk has some dynamical viscosity, η, and a shear flow $d\Omega/dr \neq 0$, then there is a torque between adjacent cylinders which can be described with

$$g = r \times 2\pi r \times \int_{-z_0}^{z_0} \Big(- \frac{d\Omega}{dr} r \Big) \eta dz = -2\pi r^3 \frac{d\Omega}{dr} \int_{-z_0}^{z_0} \eta dz. \tag{3.1}$$

The viscous interaction between the cylinders also releases thermal energy which can be described by,

$$\epsilon = \Big(r \frac{d\Omega}{dr} \Big)^2 \eta. \tag{3.2}$$

.

Let's look at the flow of mass, momentum and energy between cylinders located at r and $r + dr$. We can express the rate of accretion, the rate of the mass flow between the cylinders, as

$$\dot{M} = 2\pi r \int_{-z_0}^{z_0} \rho v_r dz = 2\pi r v_r \Sigma, \tag{3.3}$$

where v_r is a very small radial velocity. The angular momentum flow $\dot{J}$ can be expressed with

$$\dot{J} = \dot{M} j + g. \tag{3.4}$$

Here, $\dot{M}j$ gives the angular momentum carried with the mass flow, j is the angular momentum per unit mass, $j = vr = \sqrt{r^3 d\Phi/dr}$ and g gives the angular momentum transmitted by viscous forces. Finally, the energy flow can be expressed as

$$\dot{E} = \dot{M}e + g\Omega. \tag{3.5}$$

In this equation, $\dot{M}e$ gives the energy that flows with the matter while, $g\Omega$, gives the energy transmitted by viscous forces. Some energy is also dissipated as heat due to the viscosity. Because we assume that the disk is thin, we assume that the energy radiates locally from the surface of the disk at a flux rate F.

The luminosity between r and $r + dr$ is

$$\frac{dL_d}{dr} = 2\pi r \times 2F = 4\pi r F, \tag{3.6}$$

where F is the flux from unit area and $2F$ is used here since the disk radiates from both surfaces.

We can express the mass contained between r and $r + dr$ with $2\pi r\Sigma dr$ and can therefore write the equation of mass balance, eq. (2.14), as

$$\frac{\partial}{\partial t}(2\pi r\Sigma) + \frac{\partial \dot{M}}{\partial r} = 0. \tag{3.7}$$

We can then do the same thing with the angular momentum $2\pi r\Sigma j dr$ and the energy $2\pi r\Sigma e dr$, giving us the corresponding equations of angular momentum and energy balance

$$\frac{\partial}{\partial t}(2\pi r\Sigma j) + \frac{\partial \dot{J}}{\partial r} = 0, \tag{3.8}$$

and

$$\frac{\partial}{\partial t}(2\pi r\Sigma e) + \frac{\partial \dot{E}}{\partial r} + 4\pi r F = 0, \tag{3.9}$$

respectively. Note the term $4\pi r F$ in eq. (3.9). It has no equivalent in the mass and angular momentum equations since in this approximation radiation, responsible for this term, has no mass nor momentum. Similar terms appear in all three equations when using the relativistic form of the equations, but these are generally very small.

It is possible to simplify these equations using the fact that in the thin-disk approximation j, Ω, and e are all functions of radius alone, while $\Sigma, \dot{M}, \dot{J}, \dot{E}, F$, and g are functions of both radius and time. This gives

$$2\pi r \frac{\partial \Sigma}{\partial t} + \frac{\partial \dot{M}}{\partial r} = 0, \tag{3.10}$$

$$\dot{M} \frac{dj}{dr} + \frac{\partial g}{\partial r} = 0, \tag{3.11}$$

$$g \frac{d\Omega}{dr} + 4\pi r F = 0. \tag{3.12}$$

We can see from the last equation that

$$F = \frac{g}{4\pi r}\Big(-\frac{d\Omega}{dr}\Big) = \frac{1}{2}\Big(-r\frac{d\Omega}{dr}\Big)^2 \int_{-z_0}^{z_0} \eta dz, \tag{3.13}$$

if we use equation (3.1) to replace g. Earlier, ϵ, the thermal energy, was defined in equation (3.2) as $\left(r\frac{d\Omega}{dr}\right)^2 \eta$. We can then use that and simplify eq. (3.13) to

$$2F = \int_{-z_0}^{z_0} \epsilon dz. \tag{3.14}$$

The surface brightness of the disk cannot, of course, be negative. That, coupled with the fact that the angular velocity decreases with increased radius, $d\Omega/dr < 0$, and eq. (3.12) shows that the the torque cannot be negative either. If we assume that there is vacuum beyond both the outer and inner edges of the disk, the matter density falls off to 0 at both the inner and outer edges and so the torque must also be 0 there.

There must therefore be a radius r_m between the two edges of the disk, at which the torque has a maximum and thus $\partial g/\partial r = 0$. Looking at eq. (3.11), we can see that to fulfill that equation at the aforementioned radius the mass flow $\dot{M}$ must be 0 there as well. The signs on $\partial g/\partial r$ at other radii within the disk show that to fulfill eq. (3.11), $\dot{M} < 0$ for radii smaller than r_m and $\dot{M} > 0$ for radii larger than r_m. This shows that in the system described here, the disk will spread out across a wider range of radii.

Let us look at a special case: that of a steady-state, time independent accretion disk. Here $\dot{M}$ is constant both in time and radius, while other variables are dependent on radius alone. Here, integrating eq. (3.11) gives

$$g = g_0 + (-\dot{M})(j - j_0). \tag{3.15}$$

Here g_0 and j_0 are the torque and angular momentum at the inner edge of the disk, r_0. If there is no torque at r_0, then we have

$$g = (-\dot{M}_0)(j - j_0) \tag{3.16}$$

and, using eq. (3.13),

$$F = (-\dot{M})\frac{j - j_0}{4\pi r}(-\frac{d\Omega}{dr}). \tag{3.17}$$

This tells us that for steady-state accretion, the surface brightness doesn't depend on viscosity, but just the conservation laws. Looking at the equation above, we note that the surface brightness is proportional to the accretion rate and approaches 0 at both of the edges, at the inner, $j = j_0$, and of course both $1/r$ and $-d\Omega/dr$ approach 0 as r increases.

We can use eq. (3.17) to calculate the total luminosity of a steady-state accretion disk extending from r_0 to ∞ with $g_0 = 0$. Changing the variable of integration and then integrating by parts gives

$$L_d = (-\dot{M})(-e_0). \tag{3.18}$$

So the total luminosity of the disk is equal to the mass accretion rate times the energy per unit mass at the inner disk radius, r_0.

3.1 The Scale of Height

The hydrostatic equilibrium is described by

$$\frac{1}{\rho}\frac{\partial P}{\partial z} = -\frac{\partial \Phi}{\partial z}. \tag{3.19}$$

Here, P is the total pressure and is composed of gas pressure $P_{gas} = \rho c_s^2$, turbulent pressure $P_{tur} = \rho < v_t^2 >$ and radiation pressure $P_{rad} = aT^4/3$, with a being the radiation constant.

Using these definitions, the total pressure P can be written as

$$P = \rho c_s^2(1 + \epsilon^2 + \gamma^2 H) \tag{3.20}$$

with $\epsilon^2 =< v_t^2 > /c_s^2$ being the ratio between turbulent velocity and the speed of sound, and $\gamma^2 = 2aT^4/3\Sigma c_2^s$. The turbulent velocity is found by assuming that the turbulence is isotropic and using the turbulent viscosity $\nu = 1/3 < v_t >< l_t >$. Here, $< l_t >$ corresponds to the characteristic scale of the eddies. We will assume $< v_t > \simeq < l_t > \Omega$ and then use that to find the turbulent velocity,

$$\nu = \frac{1}{3}\frac{< v_t >^2}{\Omega} \Rightarrow < v_t >^2 \simeq 3\nu\Omega. \tag{3.21}$$

Thus, $\epsilon^2 = 3\nu\Omega/c_s^2$.

We define the total scale of height as

$$H = \frac{\rho}{|\frac{d\rho}{dz}|}, \tag{3.22}$$

and use eq. (3.19) to get the scale of height as a function of radius.

$$H = -\frac{dP}{d\rho}\frac{1}{g_z}. \tag{3.23}$$

Here, $g_z = -\partial\Phi_T/\partial z = GM_{bh}z/r^3 + 2\pi G\Sigma z/H$ is the vertical component of the gravity acceleration. Using that and eq. (3.20) we get the following,

$$H = \frac{\rho c_s^2(1 + \epsilon^2 + \gamma^2 H)}{2\pi G\Sigma + \Omega_K^2 H}, \tag{3.24}$$

which can be resolved for H to get,

$$H = -\frac{c_s}{\overline{Q}\omega_K}\Big((1-\beta) - \sqrt{(1-\beta)^2 + \overline{Q}^2(1+\epsilon^2)}\Big). \tag{3.25}$$

Here, $\overline{Q} = \Omega_K c_s/\pi G\Sigma$ gives the limit between a self-gravitating and keplerian regime for the scale of height, $\beta = aT^4/3\pi G\Sigma^2$ gives the relative influence of the radiative pressure with respect to the disk's self gravity [5].

3.2 The α-Disk Model

The α-disk model was first proposed by Shakura and Sunyaev (1973) [17]. It describes a thin disk ($h/r = 2z_0/r \ll 1$) with a much lower total mass than the central object, so that the disk's mass can be considered negligible.

$$\tau_{r\varphi} = \alpha\rho c_s^2 = -\alpha P. \tag{3.26}$$

Here, $\tau_{r\varphi}$ is proportional to the pressure P, with α as a dimensionless constant, c_s the speed of sound in the flow. We then have the kinematical viscosity,

$$< \nu >= \alpha c_s H, \tag{3.27}$$

where H is the scale of height, as defined in the previous section. As mentioned earlier, this model assumes a thin disk, so $H/r \ll 1$. This model is useful because we do not know much about the viscosity of accretion disks, but this replaces that unknown parameter with a single, simpler one which is $\leqslant 1$ [5].

4 The Eddington Limit

The Eddington limit is the maximum limit on the luminosity of a body while it is in hydrostatic equilibrium. If a body's luminosity exceeds that limit, the radiation pressure will be greater than the force of gravity and material from the outer layers of the body will be pushed away instead of being pulled in. This has important implications for accretion disks, whose luminosities depend on infalling matter.

Let's consider a gas element with photons moving towards the element from one direction. The gas has a scattering surface area of σ_T cm^2. The force from the radiation on one gram of gas is $F\sigma_T/c$ with F of course being the radiative flux, as in the previous chapter. The force of gravity affecting that same gram is GM/r^2 in the opposite direction. We can see that the flux where these two are equal is

$$\frac{\sigma_T}{c}F_E = \frac{GM}{r^2} \Rightarrow F_E = \frac{c}{\sigma_T}\frac{GM}{r^2}, \tag{4.1}$$

which, if the flux is spherically symmetric, gives a critical luminosity called the Eddington luminosity,

$$L_E = \frac{4\pi GMc}{\sigma_T}. \tag{4.2}$$

This luminosity can then be used to find the corresponding Eddington accretion rate,

$$L_E = \frac{GM}{r}\dot{M}_E \Rightarrow \dot{M}_E = \frac{r}{GM}L_E = \frac{4\pi rc}{\kappa}. \tag{4.3}$$

$\dot{M}_E$ limits the accretion rate. If that accretion rate is exceeded, accretion stops.

The approximate value of L_E should be noted,

$$L_E \approx 4 \cdot 10^4 \frac{M}{M_\odot}L_\odot, \tag{4.4}$$

for a fully ionized gas with σ_T on the order of 0.3 cm^2/g. [18]

5 Pseudo-Newtonian Potentials

The Newtonian potential used above is not perfectly accurate. While it is reasonable enough in many cases, in others, such as cases involving black holes, it is inadequate. An example of this can be seen when looking at gravitational fields of Newtonian objects and black holes. In the case of a Newtonian object, the gravitational acceleration towards a point mass becomes infinite at $r = 0$. In the same case for a black hole, the the gravitational acceleration reaches infinity at $r = r_g = 2GM/c^2$, as can be derived from the Schwarzchild metric in general relativity. A better approximation in this case could be made using a pseudo-Newtonian potential, in place of the Newtonian one [16],

$$\Phi_{PN} = -\frac{GM}{r - r_g}, \tag{5.1}$$

where $r_g = 2GM/c^2$ as before. This also gives,

$$\frac{d\Phi}{dr} = \frac{GM}{(r - r_g)^2}, \tag{5.2}$$

and we can find expressions for the rotational velocity, angular velocity and its derivative, specific angular momentum, and specific energy, all of which are shown below,

$$v = \sqrt{\frac{GM}{r}}\Big(\frac{r}{r - r_g}\Big), \tag{5.3}$$

$$\Omega = \sqrt{\frac{GM}{r^3}}\Big(\frac{r}{r - r_g}\Big), \tag{5.4}$$

$$\frac{d\Omega}{dr} = -\frac{3}{2}\sqrt{\frac{GM}{r^5}}\frac{(r - \frac{1}{3}r_g)r}{(r - r_g)^2}, \tag{5.5}$$

$$j = \sqrt{GMr}\Big(\frac{r}{r - r_g}\Big), \tag{5.6}$$

$$e = \Big(-\frac{GM}{2r}\Big)\frac{(r - 2r_g)r}{(r - r_g)^2}. \tag{5.7}$$

Note that the specific energy e is positive for radii $r < 2r_g$ and negative for radii $r > 2r_g$. This contrasts with the specific energy in a Newtonian potential,

$$e = \Phi_N + \frac{v^2}{2} = -\frac{GM}{2r}, \tag{5.8}$$

using $\Phi_N = -GM/r$ and $v = \sqrt{GM/r}$, where the specific energy is always negative and increases monotonically with increased radius towards 0.

Another important property can be found if we look at the derivative of the specific angular momentum j,

$$\frac{dj}{dr} = \frac{1}{2}\sqrt{\frac{GM}{r}}\frac{(r - 3r_g)r}{(r - r_g^2)^2}. \tag{5.9}$$

We see from this that j has a minimum at $r = 3r_g$. Both this and the specific energy result are the same as the results obtained in general relativity.

The minimum in angular momentum also gives us the inner edge of the accretion disk. We can see from eq. (5.5) that $d\Omega/dr < 0$ at all r and so the angular momentum is transported away from the center at all r as well. A particle in the disk will lose angular momentum and fall inwards, eventually reaching the circular orbit at $r = 3r_g$. Here it will of course continue to lose angular momentum, but there is no circular orbit possible and as a result it will fall freely towards the center.

This limit of $r = 3r_g$ only applies to a non-rotating black hole. For a rotating black hole, space around it is dragged along, allowing particles to essentially move even faster and thus allowing stable orbits closer to the event horizon. This has been seen, with some X-rays that have been measured originating much closer to the event horizon of black holes such as GX 339-4 and J1650-500. Fig. 5.1 below shows this along with graphs showing the X-ray flux, demonstrating that the flux is lowered due to the gravity of the rotating black hole [1].

An accretion disk surrounding a black hole is capable of radiating an incredible amount of energy. Going through the same same steps as in eq. (3.18) it is possible

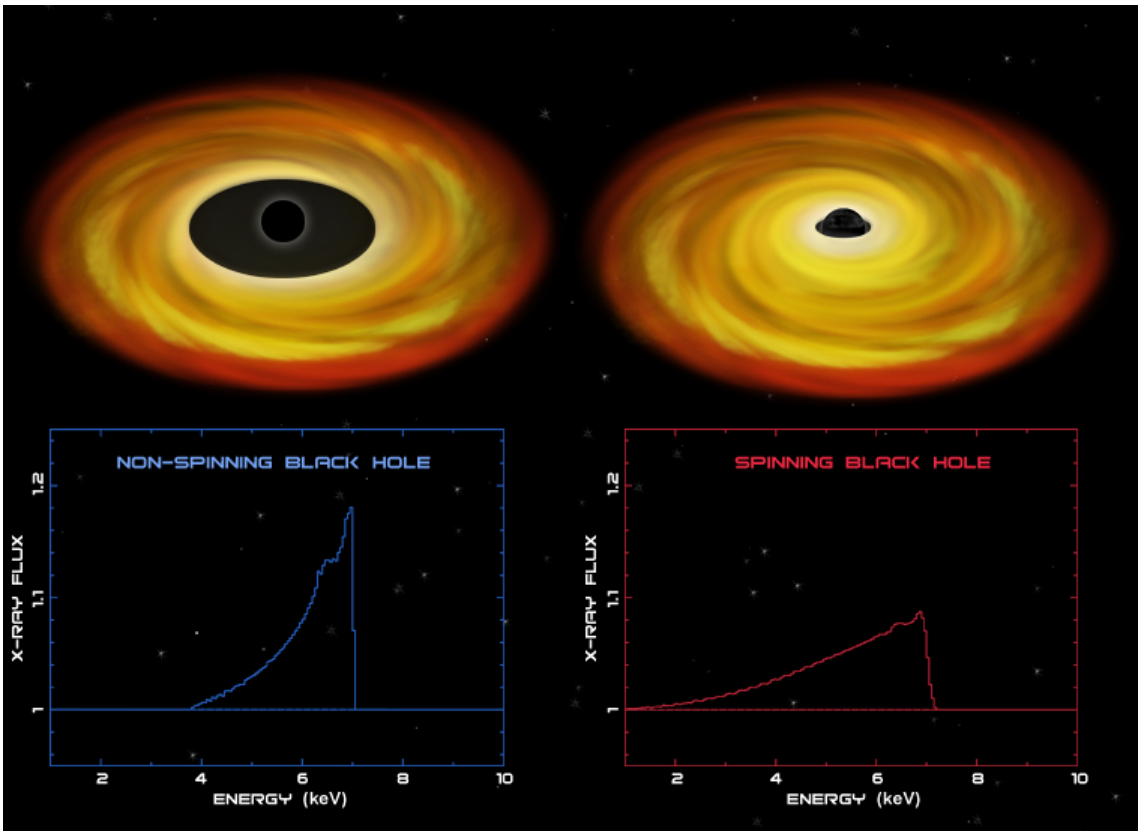

Figure 5.1: A spinning black hole allows matter to orbit much closer to the event horizon. The graphs show how X-rays from an accretion disk are shifted if the central black hole rotates. The flux of high energy X-rays is lower than for a non-rotating black hole [1].

to show the following expression for the total luminosity of the disk:

$$L_d = (-\dot{M})\frac{c^2}{16}. \tag{5.10}$$

From this equation we see that matter accreting into a schwarzschild black hole radiates 1/16 of its rest mass energy [16].

6 Black Holes and Accretion Disks

In the previous chapter we briefly looked at the case in which an accretion disk surrounds a black hole, since in those systems the pseudo-Newtonian potential becomes necessary to provide an accurate description. Here we will look more closely at those types of systems, in particular the four specific systems Cygnus X-1, SS 433, Sagittarius A and the Sombrero Galaxy, M104.

6.1 Cygnus X-1

Cygnus X-1 is a high-mass X-ray binary system consisting of a blue supergiant star and a black hole. These two bodies orbit their common center of mass every 5.6 days. This system is the brightest persistent hard X-ray source in the sky. The black hole is about 15 times the mass of the sun and spins more than 800 times per second [4].

Fig. 6.1 shows the location of Cygnus X-1 on the sky and an artist's impression of the system while fig. 6.2 shows the observed spectrum of Cygnus X-1, as well as model spectra based on models of an accretion disk, corona, and coronal reflection. Obviously, modeling a single part of the system, such as the disk, is not enough to account for the observed spectrum, but using multiple models together it is possible to get an accurate interpretation of the result [7].

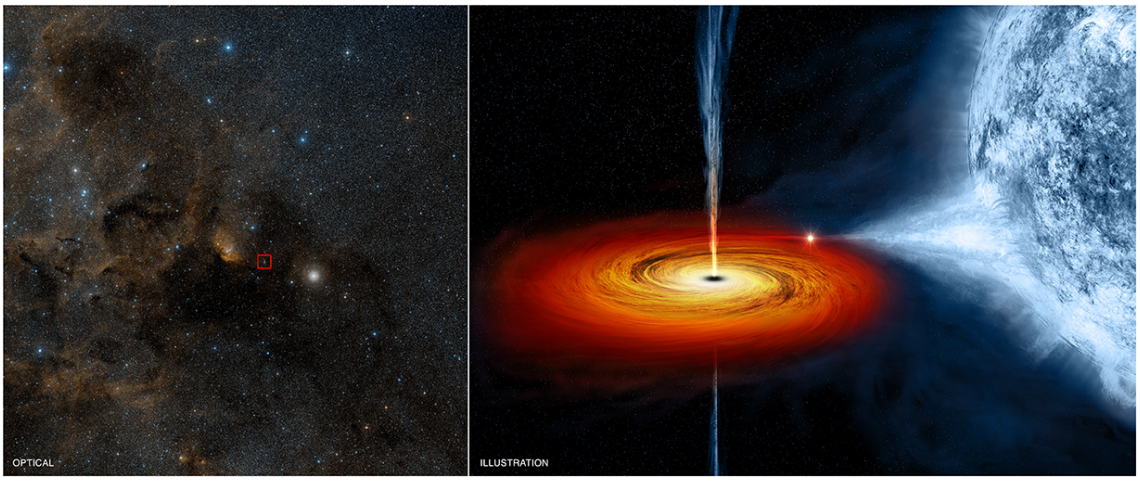

Figure 6.1: On the left, the location of Cygnus X-1 in the sky, on the right, an artist's impression of the binary system. [4]

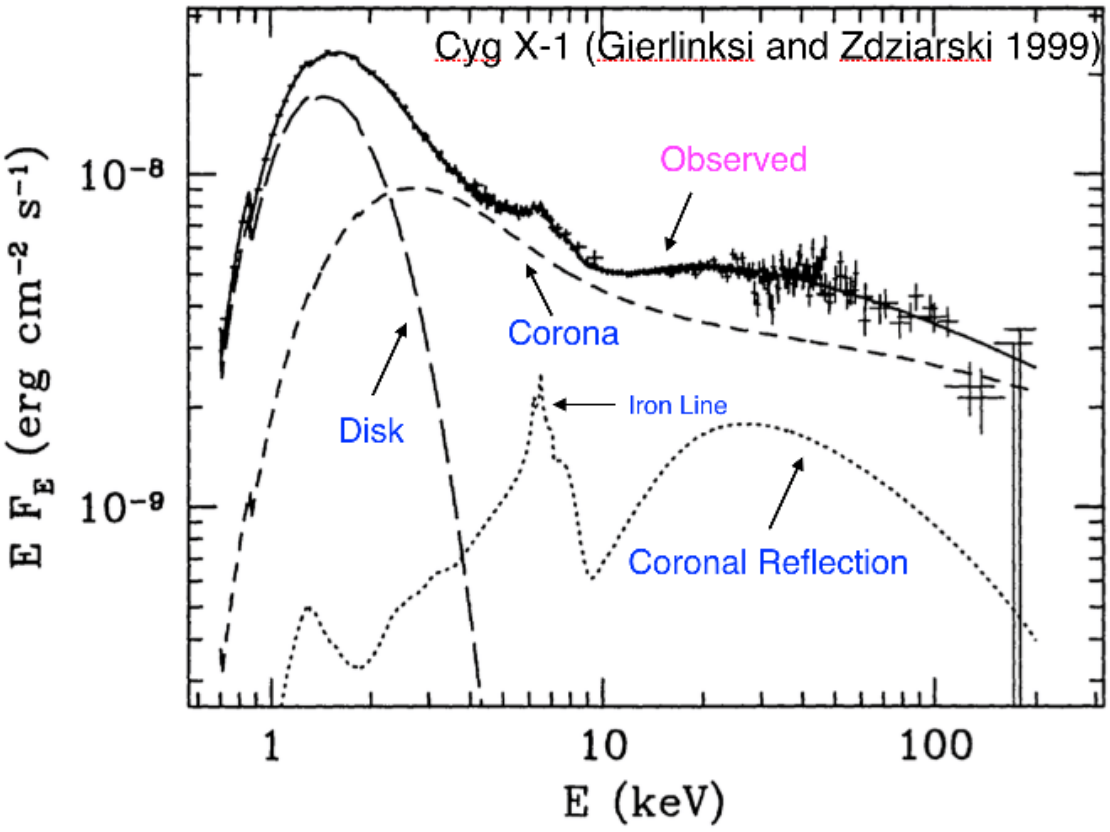

Figure 6.2: The observed flux spectrum of Cygnus X-1 along with several models demonstrating how they are accurate when combined. Note that the disk is very prominent in the X-ray region of the spectrum and most of the energy flux comes from the accretion disk. [10].

6.2 SS 433

SS 433 is a X-ray binary consisting of a primary which is either a black hole or a neutron star and an A-type star [8]. Matter is continually pulled away from the star and into an accretion disk around the compact object. Matter is hurled away from the system in two jets coming out of the compact object, perpendicular to the disk. This matter moves at around 26% of the speed of light. This system is considered one of the most exotic systems discovered due to the fact that the disk and jets precess around an axis about 20° off from the jets [8]. This means that the spectrum is both blue- and redshifted as the jets point alternately more towards us and away. Matter released by the jets forms a helix, as seen on fig. 6.3 below.

Fig. 6.5 shows the spectrum of SS 433. The horizontal lines show the rest wavelength of several lines and the location of the blue- and redshifted lines due to the jets.

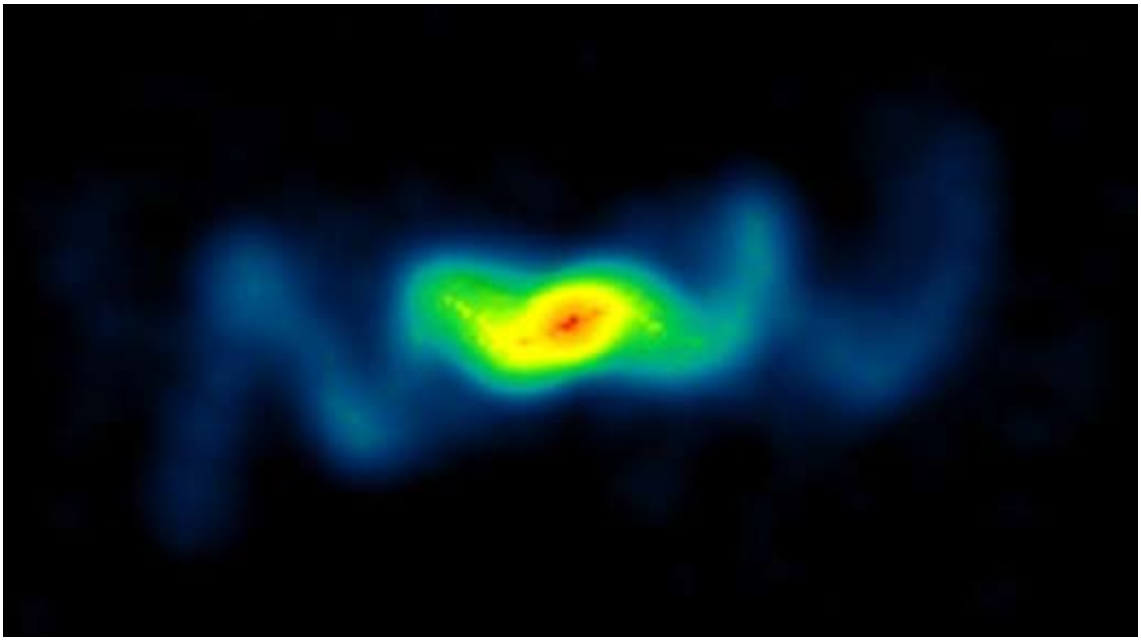

Figure 6.3: Radio image of SS 433, showing the jets [12].

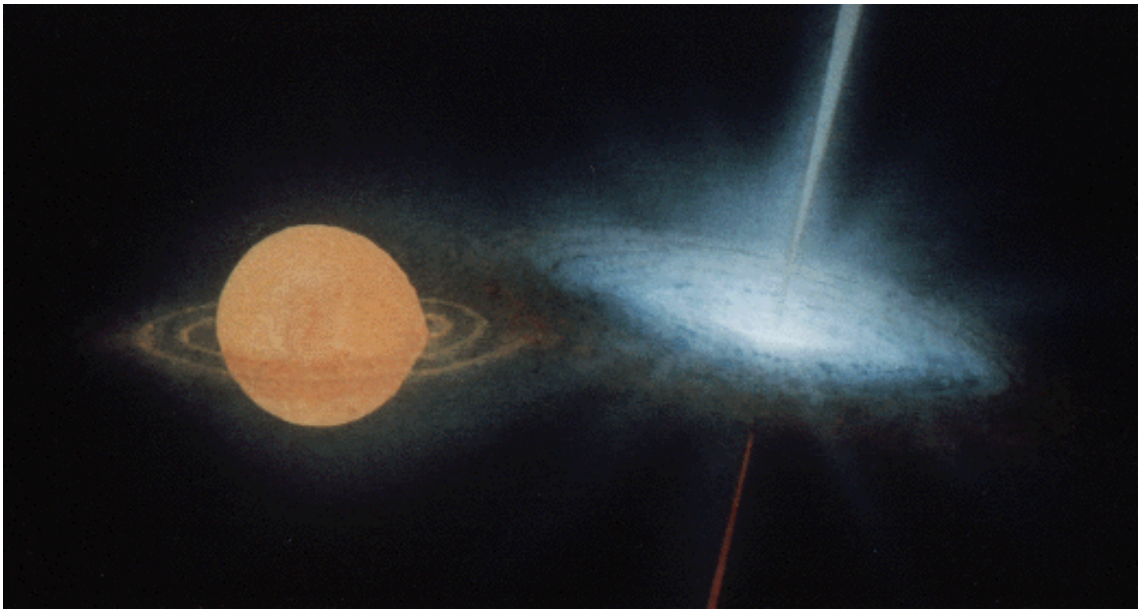

Figure 6.4: An artist's impression of SS 433 [15].

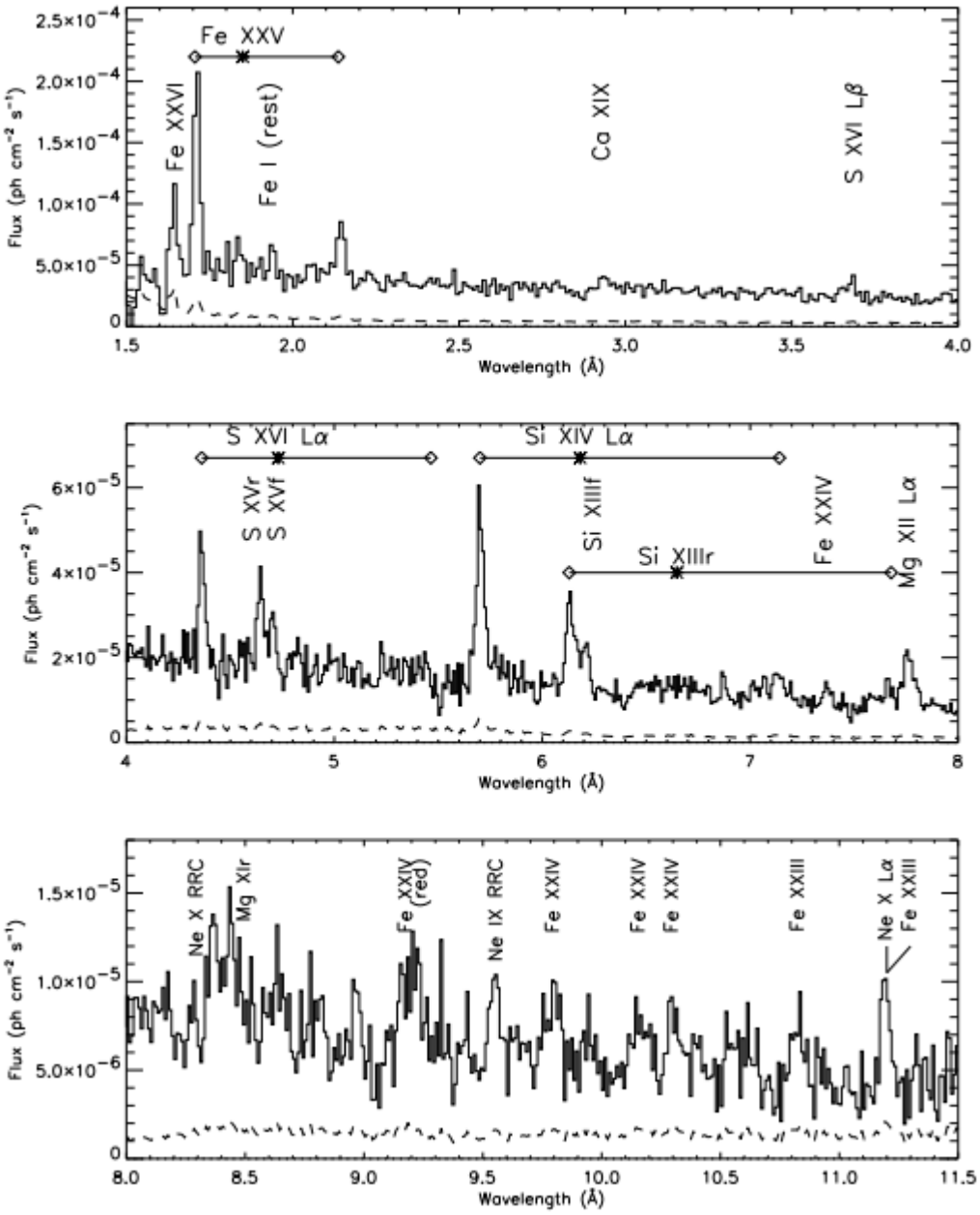

Figure 6.5: The Spectrum of SS433, observed with the Chandra High Energy Transmission Grating Spectrometer. Note the horizontal lines, which show the difference between the blue- and redshifted lines (diamonds) and the rest wavelengths (asterisks) [13].

6.3 Sagittarius A*

Sagittarius A* is the supermassive black hole at the center of the Milky Way, about 26000 light-years from Earth. Its mass is approximately 4 million solar masses. It is surprisingly faint with regards to X-rays as research has shown that less than 1% of the matter in its gravitational influence actually passes the event horizon. Most of the matter is instead ejected. This phenomenon occurs due to the heat of the accreting matter. It appears that most supermassive black holes at the center of galaxies behave like this, but Sagittarius A* is the only one where this can be observed, due to its relative proximity to Earth [3].

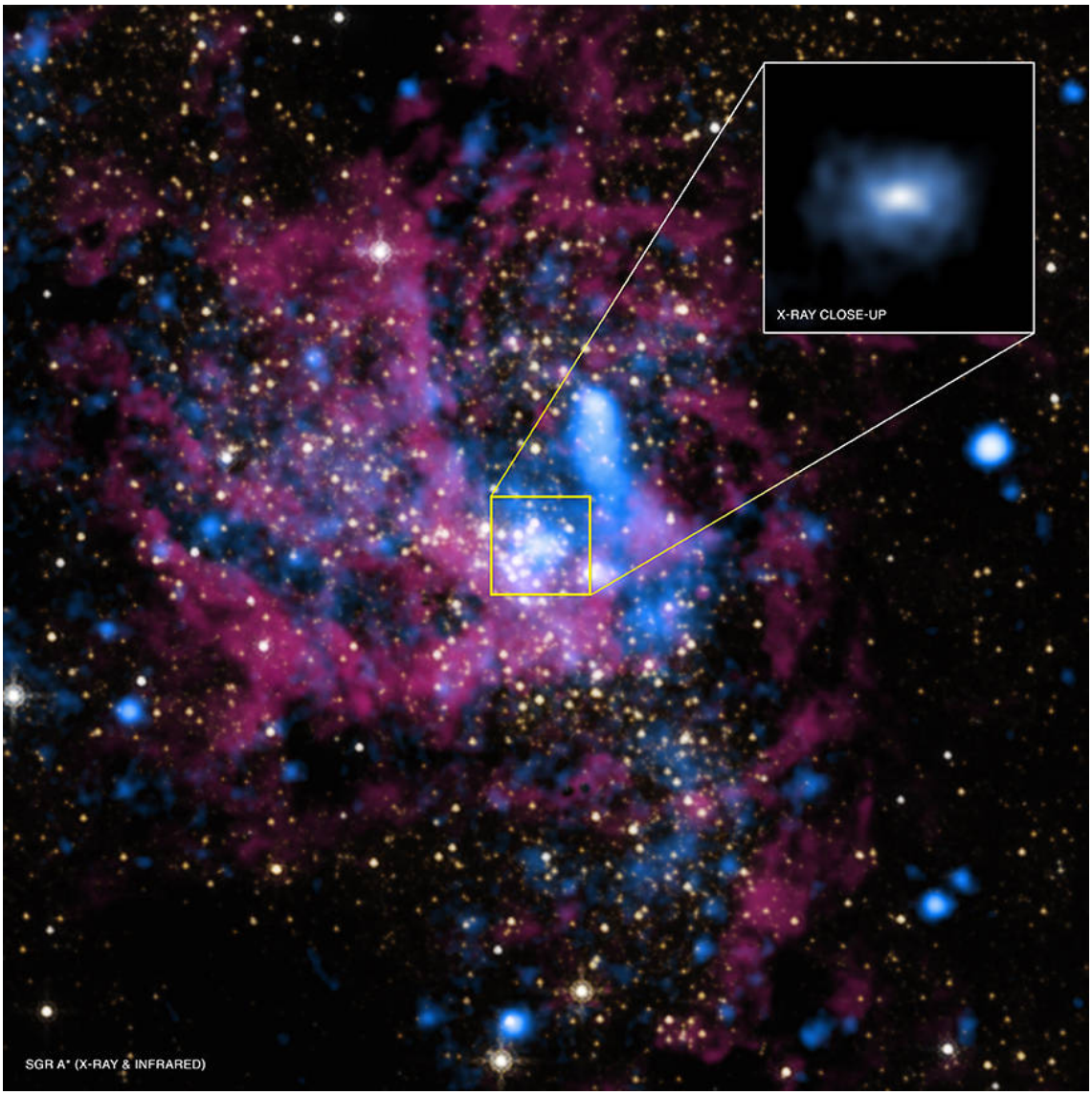

Figure 6.6: An image showing X-rays observed with Chandra in blue and infrared observed with the Hubble Space Telescope in red and yellow. The close up shows shows Sagittarius A in X-rays only [3].*

6.4 M104

The Sombrero Galaxy, also known as M104, is an unbarred spiral galaxy approximately 31 million light-years from Earth [14]. It is considerably smaller than the Milky Way, with a diameter of 50000 light-years. It has an unusually large supermassive black hole, with a mass of 1 billion solar masses [11].

M104 has a ring of dust and cold atomic hydrogen gas surrounding the galaxy's central bulge. Most of M104's star formation happens in this ring, which is visible on the figure below.[6]

Figure 6.7: Picture of M104, taken with the Hubble Space Telescope [2].

7 Summary

We have now gone through much of what is required to model an accretion disk. The process which causes a disk to form has been described, both the Roche lobe overflow in binary systems as well as the non-zero total angular momentum of the system and the collision of particles in others.

A short overview of adiabatic accretion has also been given, which neglects the loss of energy due to radiation. Following that, there was a section that analysed accretion disks using the Navier-Stokes equation of motion. We looked at the thin disk approximation and how it simplifies calculations, getting several conclusions about accretion disks in the process. The α-disk model was also described, and how it reduces a complex property, the viscosity, down to a single parameter.

The Eddington limit's implications for accretion disks were mentioned, before describing the pseudo-Newtonian potential and its uses compared to the simpler Newtonian potential.

Finally, we looked at four noteworthy systems containing black holes. Cygnus X-1, having been extensively studied, provides a lot of data on accretion disks, including giving us an example of how our accretion disk models are limited. SS 433 is an interesting system due to the disk and jets precessing around the axis of rotation. Sagittarius A* provides a look at the supermassive black holes at the center of galaxies. We also looked at M104, with its unusually large central black hole.

Bibliography

[1] Cygnus x-1, xte j1650-500, gx 339-4: "iron-clad" evidence for spinning black hole. http://chandra.harvard.edu/photo/2003/bhspin/, Visited 18. May 2017.

[2] Hubble mosaic of the majestic sombrero galaxy. http://www.spacetelescope.org/images/opo0328a/, Visited 24. May 2017.

[3] Supermassive black hole sagittarius a*. https://www.nasa.gov/mission_pages/chandra/multimedia/black-hole-SagittariusA.html, Visited 24. May 2017.

[4] J. Anderson and M. Watzke. Cygnus x-1: A stellar mass black hole. https://www.nasa.gov/mission_pages/chandra/multimedia/cygnusx1.html, Visited 18. May 2017.

[5] M. M. Armijo. Review: Accretion disk theory. Mar. 2012. https://arxiv.org/abs/1203.6851, Visited 28. May 2017.

[6] G. J. Bendo, B. A. Buckalew, D. A. Dale, B. T. Draine, R. D. Joseph, R. C. Kennicutt, Jr., K. Sheth, J.-D. T. Smith, F. Walter, D. Calzetti, J. M. Cannon, C. W. Engelbracht, K. D. Gordon, G. Helou, D. Hollenbach, E. J. Murphy, and H. Roussel. Spitzer and jcmt observations of the active galactic nucleus in the sombrero galaxy (ngc 4594). *Astrophysical Journal*, 645:134–147, 2006.

[7] E. G. Blackman and F. Nauman. Motivation and challenge to capture both large scale and local transport in next generation accretion theory. *Journal of Plasma Physics*, 81, Jan. 2015.

[8] A. Cherepashchuk. Observational manifestations of precession of accretion disk in the ss 433 binary system. *Space Science Reviews*, 102, Oct. 2002.

[9] R. Ciardullo. Binary star evolution. http://www2.astro.psu.edu/users/rbc/a1/lec16n.html, Visited 18. May 2017.

[10] M. Gierlinski and A. A. Zdziarski. Accretion disk in cyg x-1 in the soft state, 1999. ed. Juri Poutanen and Roland Svensson, ISBN: 1-886733-81-3.

[11] J. Kormendy, R. Bender, E. A. Ajhar, A. Dressler, S. M. Faber, K. Gebhardt, C. Grillmair, T. R. Lauer, D. Richstone, and S. Tremaine. Hubble space telescope spectroscopic evidence for a 1 x 10 9 msun black hole in ngc 4594. *Astrophysical Journal Letters*, 473:L91–L94, Dec. 1996.

[12] L. Krumenaker. The mystery of ss433. `http://blackholes.stardate.org/resources/article-mystery-of-ss443.html`, Visited 23. May 2017.

[13] H. L. Marshall, C. R. Canizares, and N. S. Schulz. The high resolution x-ray spectrum of ss 433 using the chandra hetgs. Sept. 2001. `https://arxiv.org/abs/astro-ph/0108206v1`, Visited 30. May 2017.

[14] K. B. W. McQuinn, E. D. Skillman, A. E. Dolphin, D. Berg, and R. Kennicutt. The distance to m104. *The Astronomical Journal*, 152(5):144, 2016.

[15] NASA. Jets from ss433. `https://apod.nasa.gov/apod/ap960306.html`, Visited 23. May 2017.

[16] J. E. Pringle. Accretion disks. *Annual Review of Astronomy and Astrophysics*, 19:137–162, 1981.

[17] N. I. Shakura and R. A. Sunyaev. Black holes in binary systems. observational appearance. *Astronomy and Astrophysics*, 24:337–355, 1973.

[18] H. C. Spruit. Accretion disks. 2000. `https://arxiv.org/abs/astro-ph/0003144v2`, Visited 30. May 2017.